Concave trisoctahedral Ag3PO4 microcrystals with high-index facets and enhanced photocatalytic properties. Chem Commun

6 AUTHORS, INCLUDING:

Zhengbo Jiao
Chinese Academy of Sciences
30 PUBLICATIONS   486 CITATIONS

SEE PROFILE

Gongxuan Lu
Chinese Academy of Sciences
227 PUBLICATIONS   5,272 CITATIONS

SEE PROFILE

Yingpu Bi
Chinese Academy of Sciences
50 PUBLICATIONS   2,603 CITATIONS

SEE PROFILE

ChemComm

COMMUNICATION

Concave trisoctahedral Ag₃PO₄ microcrystals with high-index facets and enhanced photocatalytic properties†

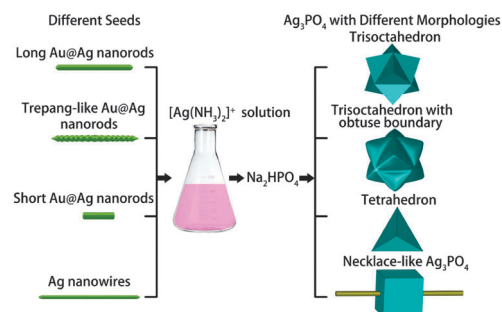Zhengbo Jiao,[a] Yan Zhang,[a] Hongchao Yu,[a] Gongxuan Lu,[a] Jinhua Ye[b] and Yingpu Bi*[a]

Herein, we demonstrate for the first time the fabrication of concave trisoctahedral Ag₃PO₄ microcrystals enclosed by {221} and {332} facets based on the heteroepitaxial growth procedure, which exhibit much higher photocatalytic activities than cubic Ag₃PO₄ and commercial N-doped TiO₂.

Semiconductor photocatalysts have attracted considerable attention during the past few decades as a result of their great potential for resolving the current energy and environmental problems.[1,2] It has been gradually acquired that the photocatalytic as well as photoelectric properties of semiconductors can be further enhanced or optimized through tailoring the morphology and the exposed crystal facets.[3–5] For example, Lu *et al.* demonstrated that anatase TiO₂ with {001} facets are more reactive than the thermodynamically stable {101} facets for the photocatalytic production of H₂ from water splitting.[6,7] Huang *et al.* reported that the {110} facets of Cu₂O exhibit higher photocatalytic activities than the {111} and {100} facets as a result of their higher surface energy.[8] More recently, our group have revealed that single-crystalline Ag₃PO₄ rhombic dodecahedrons enclosed by {110} facets exhibit much higher photocatalytic activities than cubes bound by {100} facets for the degradation of organic contaminants.[9] However, note that the as-prepared semiconductor crystals are generally bound by relatively low-index crystal planes rather than high-index facets. More specifically, the high-index facets possess the high density of atomic steps, ledges, kinks, and dangling bonds, which usually exhibit much higher chemical reaction activities than the low-index planes.[10] Although such high-index facets are fascinating and significant for the enhancement of reactivity, they usually disappear rapidly during the growth process because of their high surface energies as well as

fast growth rates. Thereby, the synthesis of semiconductor photocatalysts exposed to high-index facets and exploration of their potential applications are still a great challenge.

Herein, we demonstrate for the first time the fabrication of TOH Ag₃PO₄ microcrystals enclosed with {221} and {332} high-index facets based on the heteroepitaxial growth procedure by utilizing Au@Ag core–shell nanorods (NRs) as starting materials. Furthermore, their photocatalytic performance studies reveal that the TOH Ag₃PO₄ exhibits much higher photocatalytic properties than cubes for the degradation of organic contaminants under visible-light irradiation. The theoretical calculation suggests that Ag₃PO₄ {221} and {332} facets possess higher surface energy, which should be a significant contribution to the enhanced photocatalytic activity. Moreover, the Au@Ag nanorods embedded inside TOH Ag₃PO₄ can result in the fast separation of photoexcited electron–hole pairs from their hetero-interface and thus improve the photocatalytic efficiency.

Firstly, note that the morphology, structure, and exposed crystal facets of as-prepared Ag₃PO₄ crystals could be rationally tailored by adjusting the composition of metal starting materials. As shown in Scheme 1, Fig. S2, and Fig. S3 (ESI†), when the Au@Ag nanorods with high aspect ratio were utilized in this heteroepitaxial growth process, novel TOH Ag₃PO₄ crystals with sharp corners and edges have been fabricated. In the case of the trepang-like Au@Ag nanorods, TOH Ag₃PO₄ with an obtuse boundary could be obtained,

[a] *State Key Laboratory for Oxo Synthesis & Selective Oxidation, and National Engineering Research Center for Fine Petrochemical Intermediates, Lanzhou Institute of Chemical Physics, CAS, Lanzhou 730000, China. E-mail: yingpubi@licp.cas.cn*

[b] *International Center for Materials Nanoarchitectonics (MANA), and Research Unit for Environmental Remediation Materials, National Institute for Materials Science (NIMS), Tsukuba, 305-0047, Japan*

† Electronic supplementary information (ESI) available. See DOI: 10.1039/c2cc37324f

Scheme 1 Schematic illustration of the growth process of Ag₃PO₄ with different morphologies fabricated by the seed-mediated method using different seeds.

which possesses round edges and planes. Additionally, tetrahedral Ag_3PO_4 could be fabricated when Au@Ag nanorods with a short aspect ratio were introduced in this synthetic system. Furthermore, considering the body-centered cubic (bcc) crystalline structure and the regular tetrahedron morphology of Ag_3PO_4, it can be speculated that the tetrahedrons are bound entirely by {111} facets.[11] Moreover, in the presence of pure Ag nanowires with a length of about 10 μm, novel necklace-like Ag_3PO_4 were fabricated, and their exposed facets should be indexed to {100} facets.[12] It is well known that the metallic TOH crystal structures such as Au, Au–Pd, and Ag have been extensively fabricated by many research groups,[10,13,14] however, TOH semiconductor crystals with high index facets have rarely been reported until now as a result of their high instability. Thereby, in this work, most attention has been focused on the TOH Ag_3PO_4 to investigate the effects of high-index facets on their photo-catalytic properties.

Fig. 1A and B show the typical scanning electron microscopy (SEM) images of TOH Ag_3PO_4 microcrystals fabricated by reacting a $[Ag(NH_3)_2]^+$ complex with Na_2HPO_4 in the presence of Au@Ag nanorods. It can be clearly seen that Ag_3PO_4 microcrystals with regular concave TOH morphology have been fabricated in high yield and their dimensions are generally in the range of 1.5–2 μm (Fig. S3A, ESI†). The randomly oriented microcrystals in SEM images are consistent with the geometrical model of concave TOH when viewed from different angles, which further confirms the TOH morphology of Ag_3PO_4 microcrystals. Because no Au@Ag nanorod can be directly observed in SEM images, it could be concluded that they are embedded inside the Ag_3PO_4 microcrystals. Furthermore, the X-ray diffraction (XRD) patterns (Fig. 1C) match well with the body-centered cubic phase of Ag_3PO_4 (JCPDS. No. 06-0505) and several smaller diffraction peaks can be indexed to the facet-centered cubic (fcc) phase of Au or Ag. More specifically, the diffraction peaks of metallic Au and Ag are very similar, which cannot be obviously distinguished. Therefore, the characterization of X-ray photoelectron spectroscopy (XPS) has also been performed to further investigate their composition and clarify the existence of Au and Ag in Ag_3PO_4 microcrystals (Fig. 1D). The survey spectrum clearly confirms the presence of both gold and silver in the as-prepared product. Fig. S6 (ESI†) shows the high-resolution spectra of the TOH Ag_3PO_4 microcrystal, which gives more information about their chemical components.

Furthermore, the crystal facets of fcc metallic TOH structures, such as Au or Ag nanocrystals (NCs), have been widely investigated in recent years.[10,14] However, the crystal facets index of bcc TOH crystals has rarely been discussed so far. Although some differences exist between these two kinds of Bravais lattice, the relationship between Miller indices and projection angles should be suitable for both bcc and fcc nanocrystals because they all belong to an isometric system. Moreover, as far as the isometric system is concerned, the angles between two crystal facets have no relationship with Bravais lattice but Miller indices themselves, just as expressed as follows.[15]

$$\cos \Phi = \frac{h_1 h_2 + k_1 k_2 + l_1 l_2}{\sqrt{(h_1{}^2 + k_1{}^2 + l_1{}^2)(h_2{}^2 + k_2{}^2 + l_2{}^2)}}$$

According to the above equation, if a TOH nanocrystal is composed of a certain crystal facet, the projection angles should be confirmed. Thereby, *vice versa*, the Miller indices can be determined from the projection angles when the TOH is viewed along a certain crystallographic direction. The optimal projection direction for TOH is along [110], which results in an octagon with 2-fold symmetry.[16] The four edge-on facets can be determined by three different angles α, β and γ, and the relationship between Miller indices and the projection angles can be expressed as follows.[13,16]

$$\alpha = 180 - 2 \arctan \frac{h-1}{\sqrt{2}h}$$

$$\beta = 90 + \frac{\gamma - \alpha}{2}$$

$$\gamma = 180 - 2 \arctan \frac{1}{\sqrt{2}h}$$

Fig. 2A shows a SEM image of a single TOH Ag_3PO_4, and red lines are used to accurate the edges that form the outline of the TOH Ag_3PO_4. A model of TOH projected from the ⟨110⟩ direction has been shown in Fig. 2B, and the four edge-on facets are indicated by the black arrows. The projection angles corresponding to ideal TOH crystals enclosed by high-index facets with different Miller indices are given in Table S1 (ESI†). Comparing the measured angles with the calculated ones, it can be concluded that the four edge-on facets consist of {221} and {332} facets, which can be further confirmed by the average values of α, β and γ as shown in Fig. 2C. The inset of Fig. 2C shows an ideal model, which is made up by the average values of projection angles of ten samples ordered in the clockwise direction depending on $\alpha_1 \geq \alpha_2$ and $\gamma_1 \geq \gamma_2$. Based on the above discussion, it can be concluded that the TOH Ag_3PO_4 microcrystals are bound by high-index facets, such as {221} and {332}.

The ultraviolet visible diffuse reflectance spectrum of TOH Ag_3PO_4 has been shown in Fig. 2D, indicating that an absorbance peak edge around 550 nm has been observed. Furthermore, it exhibits stronger optical absorption at around 500–700 nm compared to cubic Ag_3PO_4, which may be due to the LSPR of gold. According to Kubelka–Munk function, the relationship between the absorption coefficient and band gap energy can be described by the equation $(\alpha h\nu)^{1/2} = A(h\nu - E_g)$, in which α, ν, A, and E_g are absorption coefficient, light frequency, proportionality constant and band gap, respectively. The plot $(\alpha h\nu)^{1/2}$ *vs.* $h\nu$ as well as the bandgap can be
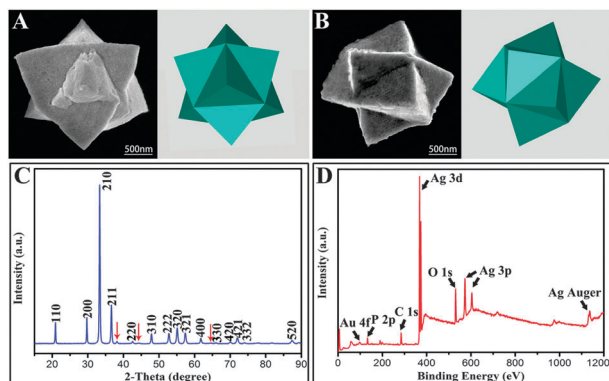

Fig. 1 (A and B) SEM images and corresponding models of TOH Ag_3PO_4 viewed along different directions. (C) XRD patterns and (D) XPS spectra of TOH Ag_3PO_4.
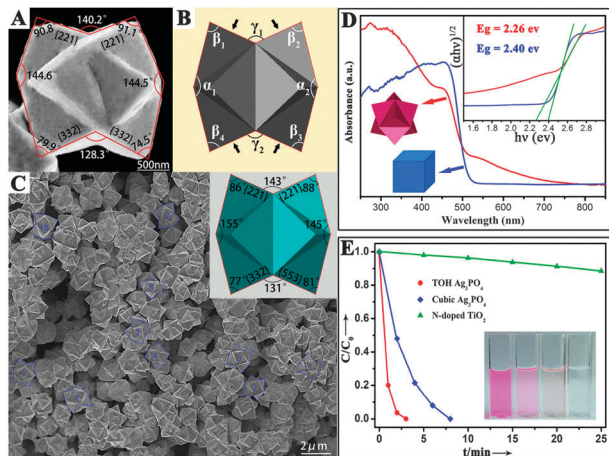
Fig. 2 (A) SEM image and (B) model of a TOH Ag$_3$PO$_4$ microcrystal viewed along the $\langle 110 \rangle$ direction. (C) SEM images of TOH Ag$_3$PO$_4$ and the inset is an ideal model fabricated by the average values of ten TOH microcrystals whose edges are highlighted by blue lines. (D) UV-vis diffusive reflectance spectra and the inset shows photographs and plots of $(\alpha h\nu)^{1/2}$ vs. $h\nu$. (E) Photocatalytic activities of TOH Ag$_3$PO$_4$ for RhB degradation under visible-light irradiation.

evaluated by extrapolating the straight line to the $h\nu$ axis intercept. As shown in the inset of Fig. 2D, the bandgap of TOH and cubic Ag$_3$PO$_4$ is 2.26 eV and 2.40 eV, respectively, indicating that the TOH structure causes the band gap narrowing.

Furthermore, the photocatalytic behaviors of TOH Ag$_3$PO$_4$ for the degradation of RhB under visible-light irradiation were explored. For comparison, the performances of cubic Ag$_3$PO$_4$ and N-doped TiO$_2$ were also investigated. As shown in Fig. 2E, except for N-doped TiO$_2$, both these Ag$_3$PO$_4$ photocatalysts exhibited excellent photocatalytic activities for the RhB degradation reaction. Although owning much larger dimensions than cubes (about 500 nm), the TOH Ag$_3$PO$_4$ microcrystals exhibited higher photocatalytic activity than cubic submicro-crystals. More specifically, the TOH Ag$_3$PO$_4$ could completely degrade RhB within 3 min, while the cubic Ag$_3$PO$_4$ needed 8 min. Moreover, it can be clearly observed that the specific surface areas of TOH Ag$_3$PO$_4$ should be much smaller than cubes as a result of their larger dimensions. Therefore, the significant difference in photocatalytic activities should not be attributed to their surface areas.

To obtain further insight into the high photocatalytic performance of TOH Ag$_3$PO$_4$, the surface structures and surface energies have also been investigated through density functional theory (DFT) calculations. The surface models of {100}, {221} and {332} facets were constructed on the basis of a slab model containing

96 atoms with a 15 Å vacuum region (Fig. 3). Each surface was scissored to form a nonpolar surface with atomic stoichiometry satisfied within the each side of the slab. Geometry relaxations were performed by fixing the midlayers. The surface energy (γ) could be computed by the formula:

$$\gamma = (E_{\text{slab}} - nE_{\text{bulk}})/2A$$

in which E_{slab} is the total energy of the slab, E_{bulk} is the total energy of the bulk per unit cell, n is the number of bulk unit cells contained in the slab and A is the surface area of each side of the slab. The calculation results showed that the surface energy of both {221} (2.01 J m^{-2}) and {332} (1.40 J m^{-2}) facets are much higher than that of {100} (1.02 J m^{-2}) facets. Correspondingly, {221} and {332} facets should be more reactive than {100} facets attributing to the presence of more defects and a higher density of unsaturated atomic steps and kinks, which can serve as active sites for breaking chemical bonds. Moreover, Au@Ag nanorods embedded inside the TOH Ag$_3$PO$_4$ could facilitate the separation of photoexcited electrons and holes, which may also contribute greatly to the enhancement of photocatalytic performance of TOH Ag$_3$PO$_4$.

In summary, we have demonstrated a facile and efficient process for the shape-selective synthesis of uniform and perfect TOH, TOH with an obtuse boundary, tetrahedron and necklace-like Ag$_3$PO$_4$ by the heteroepitaxial growth method. Importantly, there exist high-index facets, such as {221} and {332}, on the surface of TOH Ag$_3$PO$_4$, which exhibit superior photocatalytic performance for the degradation of RhB dye. This fundamental study shows a novel morphological control strategy, which may be adapted for the preparation of other semiconductor materials for photocatalytic and photoelectric applications.

Notes and references

1 J. Zhang, Q. Xu, Z. Feng, M. Li and C. Li, *Angew. Chem., Int. Ed.*, 2008, **47**, 1766.
2 F. Meng, Z. Hong, J. Arndt, M. Li, M. Zhi, F. Yang and N. Wu, *Nano Res.*, 2012, **5**, 213.
3 G. Liu, J. C. Yu, G. Q. Lu and H. M. Cheng, *Chem. Commun.*, 2011, **47**, 6763.
4 N. Wu, J. Wang, D. N. Tafen, H. Wang, J. Zheng, J. P. Lewis, X. Liu, S. S. Leonard and A. Manivannan, *J. Am. Chem. Soc.*, 2010, **132**, 6679.
5 C. Peng, T. Ke, L. Brohan, M. Richard-Plouet, J. Huang, E. Puzenat, H. Chiu and C. Lee, *Chem. Mater.*, 2008, **20**, 2426.
6 H. G. Yang, G. Liu, S. Z. Qiao, C. H. Sun, Y. G. Jin, S. C. Smith, J. Zou, H. M. Cheng and G. Q. Lu, *J. Am. Chem. Soc.*, 2009, **131**, 4078.
7 G. Liu, H. G. Yang, X. Wang, L. Cheng, J. Pan, G. Q. Lu and H. M. Cheng, *J. Am. Chem. Soc.*, 2009, **131**, 12868.
8 W. C. Huang, L. M. Lyu, Y. C. Yang and M. H. Huang, *J. Am. Chem. Soc.*, 2012, **134**, 1261.
9 Y. Bi, S. Ouyang, N. Umezawa, J. Cao and J. Ye, *J. Am. Chem. Soc.*, 2011, **133**, 6490.
10 Y. Ma, Q. Kuang, Z. Jiang, Z. Xie, R. Huang and L. Zheng, *Angew. Chem., Int. Ed.*, 2008, **47**, 8901.
11 H. Wang, Y. Bai, J. Yang, X. Lang, J. Li and L. Guo, *Chem.–Eur. J.*, 2012, **18**, 5524.
12 Y. Bi, H. Hu, S. Ouyang, Z. Jiao, G. Lu and J. Ye, *J. Mater. Chem.*, 2012, **22**, 14847.
13 Y. Yu, Q. Zhang, B. Liu and J. Y. Lee, *J. Am. Chem. Soc.*, 2010, **132**, 18258.
14 X. Xia, J. Zeng, B. McDearmon, Y. Zheng, Q. Li and Y. Xia, *Angew. Chem., Int. Ed.*, 2011, **50**, 12542.
15 R. J. D. Tilley, *Crystals and crystal structures*, John Wiley & Sons, Ltd., 2006, p. 37.
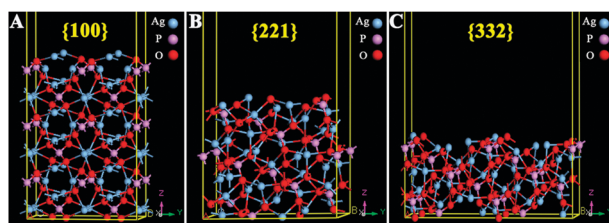16 N. Tian, Z. Y. Zhou and S. G. Sun, *J. Phys. Chem. C*, 2008, **112**, 19801.

Fig. 3 Relaxed geometries for the (A) {100}, (B) {221} and (C) {332} facets of Ag$_3$PO$_4$ based on a 96-atom slab model. The vacuum region was set as 15 Å.